Lamin A/C dysregulation contributes to cardiac pathology in a mouse model of severe spinal muscular atrophy

Darija Šoltić[1,2], Hannah K Shorrock[3], Hazel Allardyce[4], Emma L Wilson[5], Ian Holt[2], Silvia A Synowsky[6], Sally L Shirran[6], Simon H Parson[4], Thomas H Gillingwater[3], Heidi R Fuller[1,2]*

[1]Institute for Science and Technology in Medicine, Keele University, Keele ST5 5BG, UK; [2]Wolfson Centre for Inherited Neuromuscular Disease, TORCH Building, RJAH Orthopaedic Hospital, Oswestry SY10 7AG, UK; [3]Edinburgh Medical School: Biomedical Sciences, University of Edinburgh, UK; Euan MacDonald Centre for Motor Neurone Disease Research, University of Edinburgh, Edinburgh EH8 9XD, UK; [4]Institute of Education for Medical and Dental Science, College of Medicine, Medical Sciences and Nutrition, University of Aberdeen AB24 3FX, UK; [5]Chester Medical School, University of Chester, Chester CH1 4BJ, UK; [6]BSRC Mass Spectrometry and Proteomics Facility, University of St Andrews, St Andrews KY16 9ST, UK.

*Corresponding author

Wolfson Centre for Inherited Neuromuscular Disease, TORCH Building, RJAH Orthopaedic Hospital, Oswestry, SY10 7AG, UK

Email: h.r.fuller@keele.ac.uk

Telephone: +44(0)1691 404693

Fax: +44(0)1691 404065

Abstract

Cardiac pathology is emerging as a prominent systemic feature of spinal muscular atrophy (SMA), but little is known about the underlying molecular pathways. Using quantitative proteomics analysis, we demonstrate widespread molecular defects in heart tissue from the Taiwanese mouse model of severe SMA. We identify increased levels of lamin A/C as a robust molecular phenotype in the heart of SMA mice, and show that lamin A/C dysregulation is also apparent in SMA patient fibroblast cells and other tissues from SMA mice. Lamin A/C expression was regulated in-vitro by knockdown of the E1 ubiquitination factor UBA1, a key downstream mediator of SMN-dependent disease pathways, converging on β-catenin signalling. Increased levels of lamin A are known to increase the rigidity of nuclei, inevitably disrupting contractile activity in cardiomyocytes. The increased lamin A/C levels in the hearts of SMA mice therefore provide a likely mechanism explaining morphological and functional cardiac defects, leading to blood pooling. Therapeutic strategies directed at lamin A/C may therefore offer a new approach to target cardiac pathology in SMA.

Introduction

Spinal muscular atrophy (SMA) is a debilitating genetic disorder, traditionally classified as a neuromuscular disease due to the characteristic pathology of lower motor neuron degeneration and progressive muscle wasting (1). Accumulating evidence of pathology outside of the neuromuscular system, however, suggests that SMA should now be considered as a systemic condition (2). SMA has an incidence of approximately 1 in 10,000 live births (3), and in ~95% of patients it is caused by homozygous loss of *SMN1* gene, resulting in insufficient levels of the ubiquitously expressed survival of motor neuron (SMN) protein (4). There is no cure for SMA, but the last few years have seen significant progress in the development of therapies aimed at alleviating symptoms by raising full-length SMN protein levels (5). Nusinersen (Spinraza^{TM}), an antisense oligonucleotide drug, is now widely available for children and young adults with SMA, and most recently, Zolgensma^{TM} (previously known as AVXS-101), an adeno-associated virus-based gene replacement therapy, was given approval by the FDA for the treatment of SMA children under 2 years of age. Though undoubtedly an enormous step forward, none of the strategies that have been developed so far show complete efficiency (5–8). Coupled with uncertainties around long-term effectiveness and extremely high price of both strategies, there is keen interest to find alternative therapeutic strategies that could, in combination with SMN-targeted therapy, offer maximum therapeutic benefit to all SMA patients (9).

SMN perturbations influence organ development and function across multiple levels (2), and so it is likely that organ-specific and/or systemic therapy delivery may be necessary to fully rescue the SMA phenotype (5). For example, a systematic review of the literature in 2017 found 58 studies that reported on a total of 264 SMA patients with cardiac abnormalities (10). A common finding among the 77 patients with the most severe type of SMA (Type I) was

structural pathology, observed mainly in the septum and/or cardiac outflow tract. All of the 63 Type II SMA patients identified in the literature search had electrocardiogram (ECG) abnormalities, while the 124 patients with Type III SMA had cardiac rhythm disorders and/or structural abnormalities. In addition to the numerous reports of cardiac defects among SMA patients, the systematic review identified 14 studies that have documented cardiac pathology in mouse models of SMA (10). Common macroscopic findings include decreased heart size and decreased thickness of the left ventricular wall and interventricular septum, while a frequent microscopic observation was cardiac fibrosis, which was detected at a pre-symptomatic stage of the disease in both severe and intermediate mouse models of SMA (10–12). In addition, almost all studies of SMA mouse models reported bradyarrhythmias (10). A more recent study of a severe mouse model of SMA at pre- and early symptomatic time points confirmed many of these previous findings, but also noted significant pooling of blood in the heart, together with disorganization of cardiomyocytes and lack of trabecular compaction (13). These findings strongly resemble symptoms of cardiomyopathy (13), and indicate serious consequences for the normal electrical and mechanical functioning of the heart.

A recent gene-expression study of hearts from the "Taiwanese" mouse model of severe SMA identified 205 genes that were down-regulated and 269 genes that were up-regulated at an early symptomatic time-point (i.e. P5) (14). Several of these changes were tracked back to a pre-symptomatic time-point, suggesting that cardiac defects might be attributable, at least in part, to cell autonomous mechanisms (14). To the best of our knowledge, this is the first study to date that has conducted a comprehensive analysis of molecular changes in the SMA mouse heart, and whilst it has generated novel insights about changes to the transcriptome, proteomic insights into the SMA heart are lacking. This is particularly important in the

context of emerging evidence showing that the SMN protein plays fundamental roles in protein translation (15, 16). In this study, we have conducted a comprehensive quantitative proteomics study of heart tissue from the Taiwanese mouse model of severe SMA and show that there is widespread dysregulation of protein expression in SMA compared to controls. We verified the robust increase of one of these proteins, lamin A/C, in the hearts of SMA mice, and propose a role for lamin A/C in SMA cardiac pathology, strongly supported by case reports of an adult form of SMA caused by mutations in the lamin A/C encoding gene, *LMNA* (17, 18). As with a wide range of neuromuscular conditions caused by mutations in *LMNA*, including Emery-Dreifuss muscular dystrophy, limb-girdle muscular dystrophy 1B, and dilated cardiomyopathy, cardiac involvement was a notable feature in each case of *LMNA*-associated SMA. A role for lamin A/C in SMA is strengthened further by experiments in which we demonstrate dysregulation across other cells and tissues, and a mechanistic link between lamin A/C and ubiquitin-like modifier activating enzyme 1 (UBA1) protein, a key contributor to SMN-dependent disease pathways (19–21).

Results

Quantitative proteomics analysis of heart tissue from severe SMA mice reveals widespread molecular defects

To determine the molecular consequences of SMN depletion in the heart of the Taiwanese mouse model of severe SMA (22), a quantitative comparison of the SMA and age-matched control heart proteome was undertaken using iTRAQ^{TM} mass spectrometry analysis. This approach identified 3105 proteins in total (Supplementary Table 1), of which 2479 were identified with a 5% local false-discovery rate. For reliable quantification, proteins identified

from just a single peptide were removed, after which, differentially expressed proteins were identified by removal of proteins with a fold-change of less than 1.25, and finally, exclusion of proteins with a p-value of >0.05 assigned to their fold changes. This left 383 proteins that met the specified criteria for differential expression, of which 177 proteins were increased and 206 were decreased in expression in SMA mouse heart compared to controls (Supplementary Table 2). Twenty-one of the differentially expressed proteins were also altered in expression at the gene level in a recent microarray study of hearts from SMA mice at an early symptomatic time-point (i.e. P5) (14), of which 16 followed the same direction of differential expression (Supplementary Table 3).

Gene ontology (GO) analysis using the DAVID platform (23, 24) highlighted enriched biological processes and cellular components relating to the up- and down-regulated proteins, respectively (Supplementary Table 4). A relatively high proportion of up-regulated proteins were found to be blood-related (n=16), and although this compliments a previous report of blood pooling in the hearts of the Taiwanese SMA mouse model (13), these proteins were excluded from further analysis to retain focus on changes specific to the heart tissue. After also removing keratin-associated proteins (n=4), the remaining proteins were then subject to analysis using STRING 10 (25) to identify statistically significant associations between them. Comparison of the resulting networks with the GO analysis output (Supplementary Table 4) identified protein clusters associated with highly enriched molecular and/or biological processes. For the up-regulated proteins, enriched processes included organization and/or regulation of the cytoskeleton, cell junction, and extracellular matrix (Figure 1A), while clusters of down-regulated proteins were associated with translation and metabolic processes (Figure 1B).

Lamin A/C expression is dysregulated in severe SMA mice and SMA patient fibroblasts

One of the 383 differentially expressed proteins, lamin A/C, was of particular interest to us since mutations in *LMNA*, the lamin A/C encoding gene, are known to cause an adult form of SMA (17, 18). Additionally, the analysis of published proteomic studies of the neuromuscular system in SMA (26) identified lamin A/C as a conserved molecular change across three separate studies of SMA (27–29). To date, however, these findings do not appear to have been verified, nor has lamin A/C been studied in the context of SMN-dependent pathways in heart. We therefore chose to verify and understand the individual contributions of lamins A and C to the overall lamin A/C expression trend, using quantitative western blotting of heart tissue extracts from P8 SMA mice and healthy littermate controls (see workflow in Figure 2A). This analysis confirmed a robust increase in lamin A (69%, $p = 0.0007$) and C (91%, $p = 0.0079$) expression in SMA compared to control heart extracts (Figure 2B and 2C). Immunohistochemical analysis of SMA and control mouse heart sections revealed few lamin A/C positive cells in the ventricle lumen (Figure 2D), and although we cannot rule out a minor contribution, this result confirms that the increased lamin A/C levels cannot be solely attributed to circulating blood cells. Indeed, densitometry analysis of lamin A/C expression confirmed a robust upregulation of lamin A/C levels in the ventricle wall of SMA mouse heart sections compared to the unaffected controls (84%, $p = 0.0002$) (Figure 2E).

Protein extracts of SMA and control mouse brain, spinal cord, muscle, and liver tissue, as well as control and SMA patient dermal fibroblast extracts were analysed by quantitative western blotting to determine whether lamin A/C dysregulation extends beyond the heart. These analyses revealed widespread dysregulation of both lamin A and C, with differing

directions of expression change depending on the tissues examined (Figure 2B and 2C). A statistically significant reduction of lamin A levels was seen in the SMA patient fibroblast cells compared to those from healthy controls (84%, p = 0.0438), while a statistically significant upregulation of lamin A levels was found in the brain (25%, p = 0.0434) and liver (52%, p = 0.0026) tissue from SMA mice. Spinal cord extracts from SMA mice did not show a significant change in lamin A expression compared to the healthy controls, but they did show a significant increase in the levels of lamin C (43%, p = 0.0078), as did the liver (42%, p = 0.0075) and brain (43%, p= 0.0116). Patient fibroblast cells, on the contrary, showed no significant change in lamin C expression compared to the healthy controls, despite having a drastic reduction in lamin A levels. It was not possible to reliably determine whether lamin A or C were dysregulated in the skeletal muscle extracts due to large variability between samples, for reasons we are unable to explain. Lamin A dysregulation in SMA patient fibroblasts and SMA mouse heart (where protein levels were lowest, and highest, compared to controls, respectively) appears to occur post-transcriptionally, since RT-qPCR analysis showed no significant change in lamin A transcript levels in SMA compared to controls (Figure 2F).

Lamin A/C and UBA1 are mechanistically linked

Having established the widespread dysregulation of lamin A/C levels across SMA patient fibroblasts and mouse tissues (Figure 2), we next wanted to investigate whether there is a relationship between lamin A/C and UBA1. The justification for this is that a role for UBA1 in SMN-dependent pathways has been well characterised across several models of SMA (19–21), and previous research has shown that like UBA1 (19), lamin A/C is implicated in the regulation of the β-catenin signalling pathway (30, 31). In addition, a previous study reported decreased levels of UBA1 expression across a range of non-neuronal tissues from the

Taiwanese mouse model of SMA compared to controls, with the heart being most severely affected, followed by the liver (20). This is of particular interest in context with the current study, since heart tissue from SMA mice showed the greatest increase of lamin A/C levels across the tissues examined, also followed by the liver (Figure 2). (SMA patient fibroblasts appear to be an anomaly, as they were the only sample to show reduced lamin A levels compared to controls but had unchanged levels of UBA1 (Supplementary File, S4)). To investigate the relationship between lamin A/C, UBA1 and SMN, a western blot study of their relative protein expression levels was conducted using equal amounts of total protein from heart, muscle, liver, brain and spinal cord tissue extracts from healthy control mice and from healthy human fibroblasts. This revealed a strong inverse pattern of lamin A/C and UBA1 expression (Figure 3A) whereby the cells / tissues typically considered under the most mechanical strain (i.e. fibroblast cells, heart and muscle tissue) had high relative levels of lamin A/C and low relative levels of UBA1. Tissues under the least mechanical strain (i.e. liver, brain and spinal cord) showed the opposite pattern, with low relative levels of lamin A/C and high relative levels of UBA1 (Figure 3A). SMN followed the same expression trend as UBA1 across the tissues examined (Figure 3A).

Having established an inverse correlation between UBA1 and lamin A/C expression across a range of tissues, we next wanted to determine whether a mechanistic link exists between them. Knockdown of UBA1 expression in human embryonic kidney (HEK) cells resulted in a ~43% upregulation of lamin A expression ($p = 0.0398$), independent of changes to lamin C and SMN (Figure 3B). We also examined mouse embryonic fibroblast cells lacking the *LMNA* gene (32), and found that UBA1 (55%, $p = 0.0053$) and SMN (21%, $p = 0.0016$) were significantly reduced compared to the control (Figure 3C). Immunostaining of control and SMA patient fibroblasts showed colocalisation between UBA1 and lamin A at the nuclear

periphery in control and SMA cells (Figure 4A), indicating a possible interaction between lamin A/C and UBA1. To investigate this further, an immunoprecipitation from control and SMA mouse heart extracts was performed using a lamin A/C monoclonal antibody attached to magnetic beads. Although both lamin A/C and UBA1 were easily detected in SMA and control heart extracts by western blot analysis, UBA1 was undetectable in the eluates following pull-down (Figure 4B). It is important to note though that an interaction between lamin A/C and UBA1 cannot be ruled out on this basis since physiological interactions may occur between a minor proportion of the total protein present and/or it may be vulnerable to disruption by protein extraction methods (33). Interestingly, however, we did find that a small proportion of the total β-catenin co-immunoprecipitated with lamin A/C from both SMA and control heart extracts, providing evidence that lamin A/C interacts with β-catenin in the heart under normal physiological conditions (Figure 4B). When taken together, these experiments demonstrate a mechanistic link between lamin A/C and UBA1, a proven contributor to SMN-dependent disease pathways, and highlight β-catenin signalling as a potential pathway upon which they both converge.

Discussion

A small percentage of SMA cases are associated with mutations in genes other than *SMN*, including *UBA1* (34), *GARS1* (35) and *LMNA* (17, 18). Mutations in the *UBA1* gene, which encodes the UBA1 protein, cause a form of X-linked infantile SMA (SMAX2) (34), and a role for UBA1 in SMN-dependent pathways has also been well characterised across several models of SMA (19–21). Mutations in *GARS1* are known to cause infantile (36, 37) as well as an adult onset type of SMA (35). Dysregulation of UBA1/GARS1 pathways disrupted sensory neuron fate and altered sensory-motor connectivity in SMA mice, both of which were

corrected following restoration of UBA1 levels (21). Unlike *UBA1* and *GARS1*, however, the involvement of *LMNA* in SMN-dependent disease pathways has so far been unexplored. Here, we demonstrated that there are widespread molecular defects in heart tissue from the Taiwanese mouse model of severe SMA, one of which is the protein product of the *LMNA* gene, lamin A/C. We verified the robust increase of lamin A/C in the hearts from SMA mice, and have identified a mechanistic link between UBA1 and lamin A/C.

The A-type lamins, lamin A and C, are encoded by *LMNA* gene, and in addition to providing structural support to the nucleus, are involved in several other functions including mechanosignaling, chromatin organization and regulation of gene expression (38). Mutations in *LMNA* gene cause a spectrum of disorders known as laminopathies, the majority of which prominently feature cardiac pathology. The adult form of SMA caused by *LMNA* mutations is no exception to this, as each of the patients described experienced cardiac problems with disease progression and required a pacemaker. Examination of family history in each case also revealed a high frequency of cardiac abnormalities and sudden unexplained cardiac deaths (15, 16). This indisputable link between lamin A/C mutations and cardiac pathology in a wide range of conditions, including a rare form of SMA, leaves very little doubt that correct functioning of lamin A/C is a key requirement for the maintenance of cardiac health. The finding here that lamin A/C is robustly increased in heart tissue from a mouse model of SMA therefore strongly suggests that lamin A/C is responsible, at least in part, for previously reported cardiac defects in SMA.

Lamin A/C plays a significant role in the regulation of cell stability and cell dynamics (39), and its expression levels correlate with tissue stiffness, where rigid tissues have the highest levels and softer tissues the least (40). This therefore suggests that changes in lamin A/C

expression may be most pathologically relevant in SMA in highly mechanically active tissues such as the heart, where increased expression of lamin A/C is likely to impair its proper functioning. Indeed, increased rigidity of human and rat cardiomyocytes increased the extent to which cells/tissues resist deformation (i.e. passive tension) *in-vitro* (41, 42), and *in-vivo* rat experiments showed that higher passive tension slows the dynamics of myocardium contractions and induces functional heart defects (42). Increased cardiomyocyte rigidity was also identified in a cell model carrying a mutation in the *LMNA* gene (43). This mutation causes severe dilated cardiomyopathy in humans (43), which strongly mirrors the phenotype previously observed in severe and mild mouse models of SMA, including thinning of ventricle walls and interventricular septum (11, 13), and dilation of ventricles (13, 44, 45). The pathological end-point of dilated cardiomyopathy is systolic heart failure where the heart cannot pump blood properly. This would be evidenced by decreased ejection fraction and blood pooling in ventricles; both of which were identified in SMA mice (13, 44–46) and SMA patients (18, 47, 48). In the context of SMN-dependent SMA, it seems highly likely, therefore, that increased levels of lamin A/C would lead to stiffening of the cardiomyocytes, impeding their ability to contract properly and inducing the cardiac defects previously reported in SMA. In addition, cardiac fibrosis has been described in patients harbouring a LMNA mutation (49, 50), and was frequently reported in SMA patients and mouse models of SMA (10), even at a pre-symptomatic stage of the disease in both severe and intermediate mouse models of SMA (11, 12). As cardiac fibrosis is a key regulator of myocardial rigidity (42), it is therefore possible that this might further exacerbate problems described above (Figure 5).

A role for lamin A/C in SMA is strengthened further by our data demonstrating a mechanistic link between lamin A/C and UBA1, a key contributor to SMN-dependent disease pathways

(19–21). It seems highly likely that this mechanism converges on the β-catenin signalling pathway, since both lamin A/C and UBA1 are implicated in its regulation (19, 30, 31). UBA1 controls the stability of β-catenin through the canonical ubiquitin-proteasome pathway, and deficiency in UBA1 protein levels leads to β-catenin accumulation and neuromuscular pathology in SMA (19). Defective Wnt/β-catenin signalling was found to contribute to the pathology of dilated cardiomyopathy caused by mutation in *LMNA* gene (30), and in a separate study, lamin A/C was shown to regulate the differentiation fate of mesenchymal stem cells (MSCs) by controlling dynamics of the Wnt/β-catenin signalling pathway (31). Lamin A/C overexpression, for example, increased nuclear levels of β-catenin and activated the Wnt signalling pathway to promote osteoblast differentiation (31). The same study also provided evidence of an interaction between lamin A/C and β-catenin by immunoprecipitation of nuclear proteins from MSCs forcibly overexpressing lamin A/C (31). This physical interaction was proposed as a mechanism by which β-catenin is translocated to the nucleus (31). Here, we further expanded the knowledge of the relationship between lamin A/C and β-catenin, by demonstrating an interaction between them in heart extracts under normal physiological conditions.

The arguments above support the hypothesis that lamin A/C dysregulation is likely to be responsible, at least in part, for previously reported cardiac defects in SMA, but other proteins identified in this screen also offer insight into the molecular defects underlying cardiac abnormalities in SMA. For example, two such proteins, SUN domain-containing protein 2 (SUN2) (51) and cell division cycle 5-like protein (Cdc5l) (52), are known lamin A/C interactors and may provide further insights into lamin A/C-associated pathways in SMA. Like *LMNA*, mutations in *SUN2*, the gene encoding the SUN2 protein, have been associated with Emery-Dreifuss muscular dystrophy, a neuromuscular disorder often

associated with cardiac defects (53). Cdc5l, on the other hand, is a known splicing complex component that appears to require lamin A/C in order to regulate its assembly and targeting to the spliceosomal complex (52). Alterations to this interaction may therefore affect splicing and gene transcription, further exacerbating the downstream molecular consequences of reduced SMN expression. With this in mind, it is interesting to note that a large proportion of the down-regulated proteins in the SMA mouse heart were associated with translation, and re-enforces previous work showing that the SMN protein plays fundamental roles in protein translation (15, 16). It is also highly relevant that we found a large proportion of the down-regulated proteins in the SMA heart to be associated with metabolic processes, while the up-regulated proteins were strongly associated with cytoskeletal and extracellular matrix organisation (Figure 1). Imbalances in contractile performance are known to promote remodelling and dedifferentiation of adult cardiomyocytes; the consequences of which include cytoskeletal rearrangement, restructuring of contractile apparatus, and reduced oxidative metabolism (54). Ironically, it seems that these adaptive processes - presumably intended to protect the cardiomyocytes in times of mechanical and/or molecular stress – can lead to adverse consequences for the heart (54). Disruption of actin cytoskeleton, for example, can impair contractile properties of cardiomyocytes and was implicated in initiation of cardiomyocyte apoptosis (55).

Here we have offered new insight into the molecular defects underlying cardiac abnormalities in SMA, but other important questions remain that are worthy of further attention. It would be of interest in the future, for example, to explore the functional consequences of lamin A/C dysregulation in other cells and tissues throughout the natural history of disease progression in SMA. Moreover, identification of upstream regulators of lamin A/C may help to unravel the tissue-specific regulatory mechanisms that act on lamin A/C in response to SMN

depletion. Finally, and most importantly, it will be crucial to determine the extent to which SMN-replacement therapies reverse the molecular defects in SMA, and whether this is sufficient to fully rescue the cardiac defects widely reported across SMA patients and mouse models. When doing so, it would be important to monitor cardiac health longitudinally to determine whether new phenotypes emerge following long-term SMN-replacement therapy, and with increasing age. Therapies primarily designed to target neuronal tissues, such as Nusinersen, are especially relevant in this context since they are unlikely to rescue pathological defects in SMA heart. This knowledge, together with a broader understanding of the interplay between lamin A/C and other regulators of heart function in SMA, would help to isolate the most appropriate targets for therapy design that could, in combination with SMN-targeted therapy, offer maximum therapeutic benefit to all SMA patients.

Materials and Methods

Spinal muscular atrophy mouse model

The Taiwanese mouse model (original strain purchased from Jackson Laboratories, No. 005058), heterozygous for the SMN2 transgene on Smn null background (*Smn*$^{-/-}$;*SMN2*$^{tg/+}$) (22) and age-matched phenotypically normal controls (*Smn*$^{+/-}$; *SMN2*$^{tg/o}$) were maintained in SPF facilities at the University of Edinburgh. The breeding strategy, and genotyping using standard PCR protocols, were employed as previously described (56). Tissue was harvested at a symptomatic time point, postnatal day 8 (P8)**.** All animal work was carried under the appropriate Project and Personal Licenses from the UK Home Office (PPL:60/4569) and following local ethical review.

Quantitative proteomics analysis

Total protein extracts were prepared from the hearts of postnatal day 8 (P8) SMA mice (n = 5) and healthy littermate mice (n = 5) for iTRAQ quantitative mass spectrometry analysis as previously described (57). Following trypsin digestion, peptides were labelled with iTRAQ^{TM} tagging reagents according to the protocol in the iTRAQ kit and were assigned to each sample group as follows: 114-control and 115-SMA.

High pH reverse-phase liquid chromatography (RPLC) fractionation

All iTRAQ labelled peptides were combined into one tube, concentrated using a vacuum concentrator (ThermoSavant, ThermoFisher Scientific) and resuspended in 100 µl of buffer A (10 mM ammonium formate (NH_4HCO_2), 2 % acetonitrile (MeCN), pH 10.0). The peptides were then fractionated by high pH reverse-phase liquid chromatography (RPLC) using a C18 column (XBridge C18 5 µm, 4.6 x 100 mm, Waters). The column was rinsed with 96 % buffer A at 1 mL/min for 6 minutes until the optical density (OD) on the ultraviolet chromatogram returned to the baseline. The gradient ran from 4-28 % of buffer B (10 mM NH_4HCO_2, 90 % MeCN, pH 10.0) for 30 minutes to 28-50 % buffer B for 6 minutes. The column was rinsed in 80 % buffer B for 5 minutes and then was re-equilibrated at initial conditions with 4 % buffer B for 11 minutes. Fractions of 0.5 mL were collected every 30 seconds. The UV chromatogram was analysed and the fractions with similar peptide concentration across the elution profile were combined to give 12 fractions. The pooled fractions were concentrated in a vacuum concentrator and resuspended in 30 µl of 0.1 % formic acid (FA).

Liquid chromatography-tandem mass spectrometry (LC-ESI-MS/MS) analysis

One third of each fraction containing the labelled peptides was analysed by mass spectrometry. Peptides were separated by liquid chromatography (LC) using a nanoLC Ultra 2D plus loading pump and nanoLC AS-2 autosampler chromatography system (Eksigent). Peptides were loaded with buffer A (2% MeCN, 0.05% TFA in ultrapure water) and bound to an Acclaim PepMap100 trap (100 µm x 2 cm) (ThermoFisher Scientific). The trap was then washed for 10 minutes with buffer A, after which the trap was turned in-line with the analytical column (Acclaim PepMap RSLC column, 75 µm x 15 cm). The analytical solvent system consisted of buffer A and buffer B (98 % MeCN, 0.1 % FA in ultrapure water) at 300 nl/min flow rate. Peptides were eluted using the followed gradient: linear 2-20 % of buffer B over 90 minutes, linear 20-40 % of buffer B for 30 minutes, linear 40-98% of buffer B for 10 minutes, isocratic 98% of buffer B for 5 minutes, linear 98-2% of buffer B for 2.5 minutes and isocratic 2% buffer B for 12.5 minutes. The eluent was sprayed with a NANOSpray II source (electrospray ionization, ESI) into the TripleTOF 5600+ tandem mass spectrometer (AB Sciex), controlled by Analyst® TF software (AB Sciex). The mass spectrometer was operated in data-dependent acquisition (DDA) top20 positive ion mode with 120 ms acquisition time for MS (m/z 400-1250) and 80ms for MS/MS (m/z 95-1800), and 15 seconds of dynamic exclusion. MS/MS was conducted with a rolling collision energy (CE) inclusive of present iTRAQ CE adjustments.

The twelve raw mass spectrometry data files were analysed by ProteinPilot software, version 5.0.1.0 (Applied Biosystems) with the ParagonTM database search and Pro GroupTM Algorithm using the UniProtKB/Swiss-Prot FASTA database. The general Paragon search analysis parameters were: type ‘iTRAQ4plex (Peptide Labeled)’, cysteine alkylation ‘MMTS’, digestion ‘trypsin’ as the cleavage enzyme, instrument ‘TripleTOF, and species ‘Mouse’ for sample parameters; processing parameters were specified as ‘quantitative’, ‘bias

correction', 'background correction'; 'thorough ID' and 'biological modifications'. Proteins that showed a Protein Threshold > 5 were used for the Pro Group Algorithm to calculate the relative quantification of the protein expression, generating an error factor and p-value. A false discovery rate (FDR) analysis was performed using the Proteomics System Performance Evaluation Pipeline (PSPEP).

Bioinformatics analysis

The Database for Annotation, Visualization and Integrated Discovery (DAVID 6.8) (23, 24) was used for the gene ontology (GO) analysis. The analysis was performed separately for upregulated and downregulated proteins, and included terms with at least two annotated proteins and p-value ≤ 0.05. Differentially expressed proteins were also analysed using the Search Tool for the Retrieval of Interacting Genes/Proteins (STRING) 10 (25) to identify statistically significant interactions between them. Association network analysis was performed with high confidence (0.700) interaction score for upregulated and with highest confidence (0.900) interaction score for downregulated proteins to exclude false positive results.

Cell culture

Skin fibroblast cells from the Coriell Cell Repository (Supplementary File, S1) were grown in high glucose Dulbecco's Modified Eagle Medium (DMEM; Gibco) with 10% fetal bovine serum (FBS; Gibco) supplemented with 1% non-essential amino acids (MEM-NEAA; Gibco) and 1 % penicillin-streptomycin (PEN-STREP; Lonza). Wild type and *LMNA* knockout mouse embryonic fibroblast cells (MEFs) (32) were grown in DMEM (Gibco) with 15% FBS (Gibco) supplemented with 1% MEM-NEAA (Gibco) and 1 % PEN-STREP (Lonza).

HEK293 cells were obtained from European Collection of Authenticated Cell Cultures. Cell culture and knockdown of ubiquitin-like modifier-activating enzyme 1 (UBA1) was performed as previously described (21)**.** Briefly, HEK293 cells were grown in DMEM (Life Technologies) with 10% FBS (Sigma), penicillin/streptavidin (Invitrogen) and L-glutamine (Invitrogen). Cells were transfected with RNAiMax (Invitrogen) and 2.5µM Silencer Select Validated *UBA1* siRNA (s601, targeted against exons 24 and 25; Life Technologies) or 2.5µM negative control siRNA 2 (Life Technologies) according to the manufacturer's instructions. Control (CTR) and UBA1 knockdown (UBA1 KD) HEK cells were harvested 48h after transfection.

Western blotting

Protein extraction, SDS-PAGE and western blotting were performed as previously described (58). Briefly, after SDS-PAGE a part of the gel was excised and stained with Coomassie blue as an internal loading control for total protein. Proteins from the remaining part of the gel were transferred to nitrocellulose membrane by western blotting overnight. Membranes were blocked with 4% powdered milk and incubated with primary antibodies in dilution buffer (1% FBS, 1% horse serum, 0.1% BSA in PBS with 0.05% Triton X-100) for a maximum of two hours. Primary antibodies were as follows: mouse anti-SMN (MANSMA12 2E6 (59); 1:100), rabbit anti-UBA1 (Novus; NBP2-67816; 1:500-1:1000), mouse anti-lamin AC (MANLAC1 4A7 (60); 1:100) was used for cell extracts and rabbit anti-lamin AC (Abcam; ab169532; 1:2000) was used for tissue extracts. Following incubation with HRP-labelled rabbit anti-mouse Ig (DAKO, P0260) or HRP-labelled goat anti-rabbit Ig (DAKO, P0488) in dilution buffer at 0.25 ng/mL, membranes were incubated with West Pico or West Femto (Thermo Fisher) and visualised using a Gel Image Documentation system (Biorad). Densitometry measurements of antibody reactive bands were obtained using Fiji software

(v1.51) (61) and were normalised to densitometry measurements of the Coomassie stained gel. For densitometry measurements only, contrast and brightness were adjusted uniformly across the gel and blot to decrease the background and enhance signal detection.

RT-qPCR

Total RNA was extracted using RNeasy Plus Mini kit (Qiagen) and quantified with a NanoDrop ND- 1000 spectrophotometer (Thermo Fisher). Absorption ratios (OD_{260}/OD_{280} nm; OD_{260}/OD_{230} nm) were used to verify the integrity of the RNA. Total RNA was reverse transcribed using SuperScrip VILO cDNA Synthesis Kit (Invitrogen). Quantitative PCR was performed in QuantStudio 3 Real Time PCR system (Applied Biosystems), using SYBR Green detection system (SYBR Select Master Mix; Applied Biosystems). All PCR reactions were performed in triplicates and contained 3.75 ng of cDNA (fibroblast cells) or 2.8 ng of cDNA (heart tissue), and 300 nM Forward and 300 nM Reverse primers in the final volume of 20 μL. Parallel wells with no cDNA (NTC; no-template controls) were run for each gene to control for contamination. RNA Polymerase II Subunit J (*POLR2J*) and TATA-Box binding protein (*TBP*) were used as reference genes as they have previously demonstrated stable expression across tissues (62). Relative gene expression was quantified using Pfaffl method (63). The parameters of the reactions were 50°C for 2 min, 95°C for 10 min, and 40 cycles of 95°C for 15 sec and 60°C for 1 min. Dissociation curves were obtained for each sample and PCR products were run on 1% agarose gel for a quality control. Primer sequences for lamin A, *POLR2J* and *TBP* are available in the Supplementary File (S2). Efficiency of the primer pairs was determined by making serial dilutions of the cDNA, plotting the log values of the cDNA against the C_t (cycle threshold) values, and using a slope to calculate the efficiency according to the equation: $E = 10^{[-1/slope]} \times 100$ (63).

Immunohistochemistry (IHC)

SMA and control mouse hearts were fixed in 4% paraformaldehyde for 4 hours, cryopreserved in 30% sucrose solution with 0.1% sodium azide and subsequently embedded in a 1:1 solution of 30% sucrose and optimum cutting temperature compound (OCT) at -40^{o}C. Ventricular heart sections (7µm) were air dried for 1 hour and subjected to antigen retrieval by submersion for 20 minutes in 10mM sodium citrate buffer at 90°C, followed by 30 minutes cooling remaining in solution. Sections were incubated for 2 hours in blocking solution (0.4% bovine serum albumin (BSA), 1% Triton X-100 in 0.1M PBS) at 4°C and then overnight with rabbit anti-lamin A/C antibody (Novus; NBP2-19324) at 4°C. Slides were washed twice (10 minutes each in PBT (0.1M phosphate buffered saline (PBS) with 0.1% Tween-20)), followed by one 10 minute wash in 0.1M PBS. Sections were incubated with Cy3 goat anti-rabbit IgG (H+L) (ThermoFisher; A10520) for 2 hours at 4°C, with successive washes as before. Sections were mounted using MOWIOL media (10% Mowiol (Sigma; 81381), 20% glycerol, 50% 0.2M Tris buffer pH 8.5, 3% 1,4-diazobicyclooctance made up in distilled water) containing 4',6-diamidino-2-phenylindole (DAPI).

For the Figure, sections were imaged using Nikon eclipse e400 microscope (20x objective). For the purpose of quantification, sections were imaged using a Zeiss LSM710 inverted confocal microscope (63x objective). Densitometry measurements of lamin A/C staining in the heart ventricles were performed using Fiji software (version 1.51) (61). Images were calibrated to optical density (OD) as previously described (58), and rectangular selection tool of fixed size was used to measure OD of the ventricle wall. Prior to statistical analysis, the OD of the background was subtracted from the OD measurements of the ventricle wall. Nine sections from each mouse were used in the analysis.

Immunocytochemistry

Fibroblast cells were fixed in acetone: methanol solution (50:50) for 10 minutes, washed with PBS three times for five minutes and incubated with rabbit anti-UBA1 (Novus; NBP2-67816; 1:100) and mouse anti-lamin A (Santa Cruz; sc-71481; 1:50) in blocking buffer (1% FBS and 1% HS in PBS) for one or two hours. After incubation with goat anti-rabbit IgG Alexa Fluor 488 and anti-mouse IgG Alexa Fluor 546 (Life Technologies; 5 μg/mL) in blocking buffer for one hour, cells were stained with DAPI (Sigma; 0.4 μg/mL) for 10 minutes and mounted using Hydromount (National diagnostics). Between each step cells were washed with PBS three times for five minutes. Images were obtained using Leica SP5 confocal microscope with 63× oil immersion objective.

Immunoprecipitation

Immunoprecipitation was performed as described previously (64). Briefly, anti-mouse Pan Ig-coated magnetic beads (50μl) (Dynal, Oslo) were washed with 4% BSA in PBS, then incubated with an anti-lamin A/C monoclonal antibody (26) (neat, 50μl) for 1 hour at room temperature with gentle rolling. The beads were then washed and incubated for 1 hour at room temperature with RIPA extracts of heart tissue from SMA and healthy littermate control mice (15μl) on a roller. The beads were washed thoroughly with RIPA buffer before eluting captured material by heating at 90^0C for 3 minutes in 1 x SDS sample buffer (30μl) (2% sodium dodecyl sulphate- SDS, 10% glycerol, 5% 2-mercaptoethanol, 62.5 mM Tris-HCl, pH 6.8). Samples were subjected to western blotting as described above. Primary antibodies were as follows: rabbit anti-lamin AC (Abcam; ab169532; 1:2000), rabbit anti-UBA1 (Novus; NBP2-67816; 1:1000) and mouse anti-β-catenin (BD Transduction Laboratories; 610154; 1:1000).

Statistical analysis

All statistical analyses were performed in GraphPad Prism version 8.0.1 for Windows, GraphPad Software, San Diego, California USA, www.graphpad.com. The Shapiro-Wilk test was first used to assess the distribution of the data, followed by unpaired two-tailed *t*-test for parametric data, and a Mann-Whitney *U* test for a non-parametric data. All data are presented as mean +SD. Statistical significance was considered to be $p \leq 0.05$ for all analyses.

Supplementary material

Supplementary Material is available at...

Acknowledgements

The authors would like to thank Prof Colin L Stewart, Institute of Medical Biology, Singapore, for kindly providing wild type and *LMNA* knockout mouse embryonic fibroblasts, and Prof Glenn E Morris for helpful discussions about lamin A and for providing access to laboratory equipment. This research was supported by funding from the Newlife Charity [SG/15-16/11] (HF) and Keele University ACORN funding (HF & DS); British Heart Foundation [PG/16/68/31991] (IH); UK SMA Research Consortium (SMA Trust) (THG) and the Euan MacDonald Centre for Motor Neurone Disease Research (HKS and THG); and Wellcome Trust [094476/Z/10/Z] (SLS).

Conflict of interest statement

THG is a member of SMA-related advisory boards for Roche, Muscular Dystrophy UK and SMA Europe.

References

1. Groen, E.J.N., Talbot, K. and Gillingwater, T.H. (2018) Advances in therapy for spinal muscular atrophy: promises and challenges. *Nat. Rev. Neurol.*, **14**, 214–224.
2. Simone, C., Ramirez, A., Bucchia, M., Rinchetti, P., Rideout, H., Papadimitriou, D., Re, D.B. and Corti, S. (2016) Is Spinal Muscular Atrophy a disease of the motor neurons only: pathogenesis and therapeutic implications? *Cell. Mol. Life Sci.*, **73**, 1003–1020.
3. Verhaart, I.E.C., Robertson, A., Wilson, I.J., Aartsma-Rus, A., Cameron, S., Jones, C.C., Cook, S.F. and Lochmüller, H. (2017) Prevalence, incidence and carrier frequency of 5q-linked spinal muscular atrophy-a literature review. *Orphanet J. Rare Dis.*, **12**.
4. Lefebvre, S., Burglen, L., Reboullet, S., Clermont, O., Burlet, P., Viollet, L., Benichou, B., Cruaud, C., Millasseau, P., Zeviani, M., *et al.* (1995) Identification and characterization of a spinal muscular atrophy-determining gene. *Cell*, **80**, 155–165.
5. Sumner, C.J. and Crawford, T.O. (2018) Two breakthrough gene-targeted treatments for spinal muscular atrophy: challenges remain. *J. Clin. Invest.*, **128**, 3219–3227.
6. Finkel, R.S., Mercuri, E., Darras, B.T., Connolly, A.M., Kuntz, N.L., Kirschner, J., Chiriboga, C.A., Saito, K., Servais, L., Tizzano, E., *et al.* (2017) Nusinersen versus Sham Control in Infantile-Onset Spinal Muscular Atrophy. *N. Engl. J. Med.*, **377**, 1723–1732.
7. Mercuri, E., Darras, B.T., Chiriboga, C.A., Day, J.W., Campbell, C., Connolly, A.M., Iannaccone, S.T., Kirschner, J., Kuntz, N.L., Saito, K., *et al.* (2018) Nusinersen versus Sham Control in Later-Onset Spinal Muscular Atrophy. *N. Engl. J. Med.*, **378**, 625–635.
8. Mendell, J.R., Al-Zaidy, S., Shell, R., Arnold, W.D., Rodino-Klapac, L.R., Prior, T.W., Lowes, L., Alfano, L., Berry, K., Church, K., *et al.* (2017) Single-Dose Gene-Replacement Therapy for Spinal Muscular Atrophy. *N. Engl. J. Med.*, **377**, 1713–1722.
9. Bowerman, M. (2019) Funding for spinal muscular atrophy research must continue. *Futur.*

Neurol, **14**.

10. Wijngaarde, C.A., Blank, A.C., Stam, M., Wadman, R.I., Van Den Berg, L.H. and Van Der Pol, W.L. (2017) Cardiac pathology in spinal muscular atrophy: a systematic review. *Orphanet J. Rare Dis.*, **12**.
11. Shababi, M., Habibi, J., Yang, H.T., Vale, S.M., Sewell, W.A. and Lorson, C.L. (2010) Cardiac defects contribute to the pathology of spinal muscular atrophy models. *Hum. Mol. Genet.*, **19**, 4059–4071.
12. Cobb, M.S., Rose, F.F., Rindt, H., Glascock, J.J., Shababi, M., Miller, M.R., Osman, E.Y., Yen, P.-F., Garcia, M.L., Martin, B.R., *et al.* (2013) Development and characterization of an SMN2-based intermediate mouse model of Spinal Muscular Atrophy. *Hum. Mol. Genet.*, **22**, 1843–1855.
13. Maxwell, G.K., Szunyogova, E., Shorrock, H.K., Gillingwater, T.H. and Parson, S.H. (2018) Developmental and degenerative cardiac defects in the Taiwanese mouse model of severe spinal muscular atrophy. *J. Anat.*, **232**, 965–978.
14. Sheng, L., Wan, B., Feng, P., Sun, J., Rigo, F., Bennett, C.F., Akerman, M., Krainer, A.R. and Hua, Y. (2018) Downregulation of Survivin contributes to cell-cycle arrest during postnatal cardiac development in a severe spinal muscular atrophy mouse model. *Hum. Mol. Genet.*, **27**, 486–498.
15. Sanchez, G., Dury, A.Y., Murray, L.M., Biondi, O., Tadesse, H., El Fatimy, R., Kothary, R., Charbonnier, F., Khandjian, E.W. and Côté, J. (2013) A novel function for the survival motoneuron protein as a translational regulator. *Hum. Mol. Genet.*, **22**, 668–684.
16. Bernabò, P., Tebaldi, T., Groen, E.J.N., Quattrone, A., Gillingwater, T.H. and Viero, G. (2017) In Vivo Translatome Profiling in Spinal Muscular Atrophy Reveals a Role for SMN Protein in Ribosome Biology. *Cell Rep.*, **21**, 953–965.

17. Rudnik-Schöneborn, S., Botzenhart, E., Eggermann, T., Senderek, J., Schoser, B.G.H., Schröder, R., Wehnert, M., Wirth, B. and Zerres, K. (2007) Mutations of the LMNA gene can mimic autosomal dominant proximal spinal muscular atrophy. *Neurogenetics*, **8**, 137–142.

18. Iwahara, N., Hisahara, S., Hayashi, T., Kawamata, J. and Shimohama, S. (2015) A novel lamin A/C gene mutation causing spinal muscular atrophy phenotype with cardiac involvement: report of one case. *BMC Neurol.*, **15**, 269.

19. Wishart, T.M., Mutsaers, C.A., Riessland, M., Reimer, M.M., Hunter, G., Hannam, M.L., Eaton, S.L., Fuller, H.R., Roche, S.L., Somers, E., *et al.* (2014) Dysregulation of ubiquitin homeostasis and β-catenin signaling promote spinal muscular atrophy. *J. Clin. Invest.*, **124**, 1821–1834.

20. Powis, R.A., Karyka, E., Boyd, P., Côme, J., Jones, R.A., Zheng, Y., Szunyogova, E., Groen, E.J.N., Hunter, G., Thomson, D., *et al.* (2016) Systemic restoration of UBA1 ameliorates disease in spinal muscular atrophy. *JCI Insight*, **1**, e87908.

21. Shorrock, H.K., Van Der Hoorn, D., Boyd, P.J., Llavero Hurtado, M., Lamont, D.J., Wirth, B., Sleigh, J.N., Schiavo, G., Wishart, T.M., Groen, E.J.N., *et al.* (2018) UBA1/GARS-dependent pathways drive sensory-motor connectivity defects in spinal muscular atrophy. *Brain*, **141**, 2878–2894.

22. Hsieh-Li, H.M., Chang, J.-G., Jong, Y.-J., Wu, M.-H., Wang, N.M., Tsai, C.H. and Li, H. (2000) A mouse model for spinal muscular atrophy. *Nat. Genet.*, **24**, 66–70.

23. Huang, D.W., Sherman, B.T. and Lempicki, R.A. (2009) Systematic and integrative analysis of large gene lists using DAVID bioinformatics resources. *Nat. Protoc.*, **4**, 44–57.

24. Huang, D.W., Sherman, B.T. and Lempicki, R.A. (2009) Bioinformatics enrichment tools: paths toward the comprehensive functional analysis of large gene lists. *Nucleic*

Acids Res., **37**, 1–13.

25. Szklarczyk, D., Franceschini, A., Wyder, S., Forslund, K., Heller, D., Huerta-Cepas, J., Simonovic, M., Roth, A., Santos, A., Tsafou, K.P., *et al.* (2015) STRING v10: protein–protein interaction networks, integrated over the tree of life. *Nucleic Acids Res.*, **43**.
26. Fuller, H.R., Gillingwater, T.H. and Wishart, T.M. (2016) Commonality amid diversity: Multi-study proteomic identification of conserved disease mechanisms in spinal muscular atrophy. *Neuromuscul. Disord.*, **26**, 560–569.
27. Mutsaers, C.A., Lamont, D.J., Hunter, G., Wishart, T.M. and Gillingwater, T.H. (2013) Label-free proteomics identifies Calreticulin and GRP75/Mortalin as peripherally accessible protein biomarkers for spinal muscular atrophy. *Genome Med*, **5**.
28. Aghamaleky Sarvestany, A., Hunter, G., Tavendale, A., Lamont, D.J., Hurtado, M.L., Graham, L.C., Wishart, T.M. and Gillingwater, T.H. (2014) Label-Free Quantitative Proteomic Profiling Identifies Disruption of Ubiquitin Homeostasis As a Key Driver of Schwann Cell Defects in Spinal Muscular Atrophy. *J. Proteome Res.*, **13**, 4546–4557.
29. Fuller, H.R., Mandefro, B., Shirran, S.L., Gross, A.R., Kaus, A.S., Botting, C.H., Morris, G.E. and Sareen, D. (2016) Spinal Muscular Atrophy Patient iPSC-Derived Motor Neurons Have Reduced Expression of Proteins Important in Neuronal Development. *Front. Cell. Neurosci.*, **9**, 506.
30. Le Dour, C., Macquart, C., Sera, F., Homma, S., Bonne, G., Morrow, J.P., Worman, H.J. and Muchir, A. (2017) Decreased WNT/b-catenin signalling contributes to the pathogenesis of dilated cardiomyopathy caused by mutations in the lamin a/C gene. *Hum. Mol. Genet.*, **26**, 333–343.
31. Bermeo, S., Vidal, C., Zhou, H. and Duque, G. (2015) Lamin A/C Acts as an Essential Factor in Mesenchymal Stem Cell Differentiation Through the Regulation of the Dynamics of the Wnt/β-Catenin Pathway. *J. Cell. Biochem.*, **116**, 2344–2353.

32. Sullivan, T., Escalante-Alcalde, D., Bhatt, H., Anver, M., Bhat, N., Nagashima, K., Stewart, C.L. and Burke, B. (1999) Loss of A-type Lamin Expression Compromises Nuclear Envelope Integrity Leading to Muscular Dystrophy. *J. Cell Biol.*, **147**, 913–919.

33. Kubben, N., Voncken, J.W., Demmers, J., Calis, C., van Almen, G., Pinto, Y. and Misteli, T. (2010) Identification of differential protein interactors of lamin A and progerin. *Nucleus*, **1**, 513–525.

34. Ramser, J., Ahearn, M.E., Lenski, C., Yariz, K.O., Hellebrand, H., von Rhein, M., Clark, R.D., Schmutzler, R.K., Lichtner, P., Hoffman, E.P., *et al.* (2008) Rare Missense and Synonymous Variants in UBE1 Are Associated with X-Linked Infantile Spinal Muscular Atrophy. *Am. J. Hum. Genet.*, **82**, 188–193.

35. Antonellis, A., Ellsworth, R.E., Sambuughin, N., Puls, I., Abel, A., Lee-Lin, S.-Q., Jordanova, A., Kremensky, I., Christodoulou, K., Middleton, L.T., *et al.* (2003) Glycyl tRNA synthetase mutations in Charcot-Marie-Tooth disease type 2D and distal spinal muscular atrophy type V. *Am. J. Hum. Genet.*, **72**, 1293–1299.

36. Sivakumar, K., Kyriakides, T., Puls, I., Nicholson, G.A., Funalot, B., Antonellis, A., Sambuughin, N., Christodoulou, K., Beggs, J.L., Zamba-Papanicolaou, E., *et al.* (2005) Phenotypic spectrum of disorders associated with glycyl-tRNA synthetase mutations. *Brain*, **128**, 2304–2314.

37. James, P.A., Cader, M.Z., Muntoni, F., Childs, A.-M., Crow, Y.J. and Talbot, K. (2006) Severe childhood SMA and axonal CMT due to anticodon binding domain mutations in the GARS gene. *Neurology*, **67**, 1710–2.

38. Naetar, N., Ferraioli, S. and Foisner, R. (2017) Lamins in the nuclear interior − life outside the lamina. *J. Cell Sci.*, **130**, 2087–2096.

39. Harada, T., Swift, J., Irianto, J., Shin, J.W., Spinler, K.R., Athirasala, A., Diegmiller, R., Dingal, P.C.D.P., Ivanovska, I.L. and Discher, D.E. (2014) Nuclear lamin stiffness is a

barrier to 3D migration, but softness can limit survival. *J. Cell Biol.*, **204**, 669–682.

40. Swift, J., Ivanovska, I.L., Buxboim, A., Harada, T., Dingal, P.C.D.P., Pinter, J., Pajerowski, J.D., Spinler, K.R., Shin, J.-W., Tewari, M., *et al.* (2013) Nuclear Lamin-A Scales with Tissue Stiffness and Enhances Matrix-Directed Differentiation. *Science*, **341**, 965–966.
41. Borbély, A., Van Der Velden, J., Papp, Z., Bronzwaer, J.G.F., Edes, I., Stienen, G.J.M. and Paulus, W.J. (2005) Cardiomyocyte Stiffness in Diastolic Heart Failure. *Circulation*, **111**, 774–781.
42. Røe, A.T., Magnus Aronsen, J., Skårdal, K., Hamdani, N., Linke, W.A., Danielsen, H.E., Sejersted, O.M., Sjaastad, I. and Louch, W.E. (2017) Increased passive stiffness promotes diastolic dysfunction despite improved Ca2+ handling during left ventricular concentric hypertrophy. *Cardiovasc. Res.*, **113**, 1161–1172.
43. Lanzicher, T., Martinelli, V., Puzzi, L., Del Favero, G., Codan, B., Long, C.S., Mestroni, L., Taylor, M.R.G. and Sbaizero, O. (2015) The Cardiomyopathy Lamin A/C D192G Mutation Disrupts Whole-Cell Biomechanics in Cardiomyocytes as Measured by Atomic Force Microscopy Loading-Unloading Curve Analysis. *Sci. Reports* , **5**.
44. Heier, C.R., Satta, R., Lutz, C. and Didonato, C.J. (2010) Arrhythmia and cardiac defects are a feature of spinal muscular atrophy model mice. *Hum. Mol. Genet.*, **19**, 3906–3918.
45. Bogdanik, L.P., Osborne, M.A., Davis, C., Martin, W.P., Austin, A., Rigo, F., Frank Bennett, C. and Lutz, C.M. (2015) Systemic, postsymptomatic antisense oligonucleotide rescues motor unit maturation delay in a new mouse model for type II/III spinal muscular atrophy. *PNAS*, **112**, E5863–E5872.
46. Shababi, M., Habibi, J., Ma, L., Glascock, J.J., Sowers, J.R. and Lorson, C.L. (2012) Partial restoration of cardio-vascular defects in a rescued severe model of spinal muscular atrophy. *J. Mol. Cell. Cardiol.*, **52**, 1074–1082.

47. Yasuma, F., Kuru, S. and Konagaya, M. (2004) Dilated Cardiomyopathy in Kugelberg-Welander Disease: Coexisting Sleep Disordered Breathing and Its Treatment with Continuous Positive Airway Pressure. *Intern. Med.*, **43**, 951–954.

48. Roos, M., Sarkozy, A., Chierchia, G.B., De Wilde, P., Schmedding, E. and Brugada, P. (2009) Malignant Ventricular Arrhythmia in a Case of Adult Onset of Spinal Muscular Atrophy (Kugelberg-Welander Disease). *J Cardiovasc Electrophysiol*, **20**, 342–344.

49. Le Dour, C., Wu, W., Béréziat, V., Capeau, J., Vigouroux, C. and Worman, H.J. (2017) Extracellular matrix remodeling and transforming growth factor-β signaling abnormalities induced by lamin A/C variants that cause lipodystrophy. *J. Lipid Res.*, **58**, 151–163.

50. van Tintelen, J.P., Tio, R.A., Kerstjens-Frederikse, W.S., van Berlo, J.H., Boven, L.G., Suurmeijer, A.J.H., White, S.J., den Dunnen, J.T., te Meerman, G.J., Vos, Y.J., *et al.* (2007) Severe Myocardial Fibrosis Caused by a Deletion of the 5' End of the Lamin A/C Gene. *J. Am. Coll. Cardiol.*, **49**, 2430–2439.

51. Taranum, S., Vaylann, E., Meinke, P., Abraham, S., Yang, L., Neumann, S., Karakesisoglou, I., Wehnert, M. and Noegel, A.A. (2012) LINC complex alterations in DMD and EDMD/CMT fibroblasts. *Eur. J. Cell Biol.*, **91**, 614–628.

52. Zahr, H.C. and Jaalouk, D.E. (2018) Exploring the Crosstalk Between LMNA and Splicing Machinery Gene Mutations in Dilated Cardiomyopathy. *Front. Genet*, **9**.

53. Meinke, P., Mattioli, E., Haque, F., Antoku, S., Columbaro, M., Straatman, K.R., Worman, H.J., Gundersen, G.G., Lattanzi, G., Wehnert, M., *et al.* (2014) Muscular Dystrophy-Associated SUN1 and SUN2 Variants Disrupt Nuclear-Cytoskeletal Connections and Myonuclear Organization. *PLoS Genet.* , **10**, e1004605.

54. Szibor, M., Pöling, J., Warnecke, H., Kubin, T. and Braun, T. (2014) Remodeling and dedifferentiation of adult cardiomyocytes during disease and regeneration. *Cell. Mol.*

Life Sci, **71**, 1907–1916.

55. Communal, C., Sumandea, M., de Tombe, P., Narula, J., Solaro, R.J. and Hajjar, R.J. (2002) Functional consequences of caspase activation in cardiac myocytes. *PNAS*, **99**, 6252–6256.

56. Riessland, M., Ackermann, B., Forster, A., Jakubik, M., Hauke, J., Garbes, L., Fritzsche, I., Mende, Y., Blumcke, I., Hahnen, E., *et al.* (2010) SAHA ameliorates the SMA phenotype in two mouse models for spinal muscular atrophy. *Hum. Mol. Genet.*, **19**, 1492–1506.

57. Fuller, H.R., Hurtado, M.L., Wishart, T.M. and Gates, M.A. (2014) The rat striatum responds to nigro-striatal degeneration via the increased expression of proteins associated with growth and regeneration of neuronal circuitry. **12**.

58. Šoltić, D., Bowerman, M., Stock, J., Shorrock, H.K., Gillingwater, T.H. and Fuller, H.R. (2018) Multi-Study Proteomic and Bioinformatic Identification of Molecular Overlap between Amyotrophic Lateral Sclerosis (ALS) and Spinal Muscular Atrophy (SMA). *Brain Sci.*, **8**.

59. Young, P.J., Le, T.T., thi Man, N., Burghes, A.H.M. and Morris, G.E. (2000) The Relationship between SMN, the spinal muscular atrophy protein, and nuclear coiled bodies in differentiated tissues and cultured cells. *Exp. Cell Res.*, **256**, 365–374.

60. Manilal, S., Randles, K.N., Aunac, C., Nguyen, M. thi and Morris, G.E. (2004) A lamin A/C beta-strand containing the site of lipodystrophy mutations is a major surface epitope for a new panel of monoclonal antibodies. *Biochim. Biophys. Acta*, **1671**, 87–92.

61. Schindelin, J., Arganda-Carreras, I., Frise, E., Kaynig, V., Longair, M., Pietzsch, T., Preibisch, S., Rueden, C., Saalfeld, S., Schmid, B., *et al.* (2012) Fiji: an open-source platform for biological-image analysis. *Nat. Methods*, **9**, 676–682.

62. Radonić, A., Thulke, S., Mackay, I.M., Landt, O., Siegert, W. and Nitsche, A. (2004)

Guideline to reference gene selection for quantitative real-time PCR. *Biochem. Biophys. Res. Commun.*, **313**, 856–62.

63. Pfaffl, M.W. (2001) A new mathematical model for relative quantification in real-time RT-PCR. *Nucleic Acids Res.*, **29**, e45.

64. Fuller, H.R., Marani, L., Holt, I., Woodhams, P.L., Webb, M.M. and Gates, M.A. (2017) Monoclonal antibody Py recognizes neurofilament heavy chain and is a selective marker for large diameter neurons in the brain. *Brain Struct. Funct.*, **222**, 867–879.

Figure 1. Bioinformatics analysis of the proteins dysregulated in heart tissue from SMA mice. A) Upregulated proteins (n=177) and B) downregulated proteins (n=206) were subjected to STRING 10 analysis. Of these, 103 upregulated and 91 downregulated proteins are not shown as statistically significant interactions were not identified in STRING 10. Protein associations were identified with high confidence (0.700) interaction score for A) upregulated and with the highest confidence (0.900) interaction score for B) downregulated proteins. The thickness and colour of the lines indicate confidence of the interaction (see legend inset in figure). Protein networks were compared to the GO analysis output (Supplementary Table 4). The analysis identified protein clusters that associate with enriched GO terms in the cellular component (black) and biological process (red) domain. Proteins annotated to each term are shown in corresponding circles.

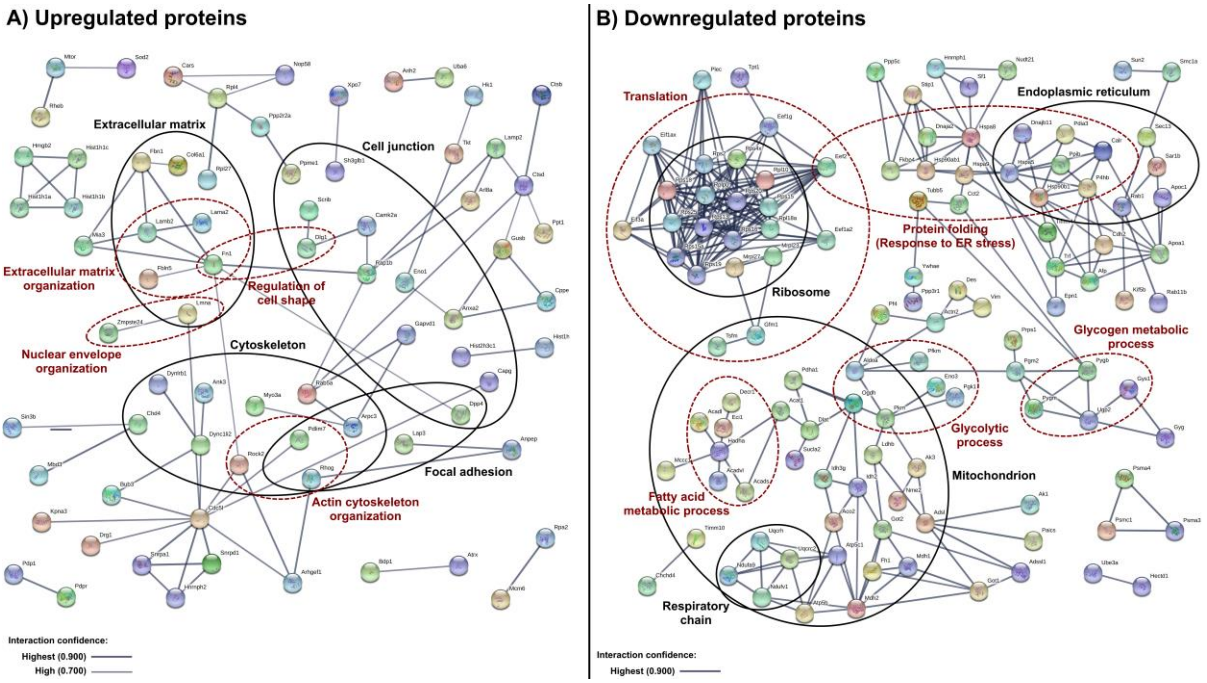

Figure 2. Widespread dysregulation of lamin A/C expression in fibroblasts from SMA patients and in tissues from SMA mice (P8) A) Schematic diagram showing the quantitative western blot analysis workflow. Total protein extracts from human fibroblast cells and mouse tissues were subjected to SDS-PAGE. A part of the gel was stained with Coomassie blue as an internal, total protein loading control. Proteins from the remaining part of the gel were transferred to nitrocellulose membrane and developed with the appropriate antibody. Quantification of protein levels was performed by normalising densitometry measurements of antibody reactive bends to densitometry measurements of Coomassie stained gel. Image created with BioRender.com. B**)** Representative western blots showing lamin A/C protein levels in the heart, spinal cord, brain, liver and muscle tissue from SMA mice (n=5) and healthy controls (n = 5), and in fibroblast cells from SMA patients (n = 3) and age matched male healthy controls (n = 3). Fibroblast cells are listed in this order: 1. GM00498, 2. GM05659, 3. GM00302, 4. GM03813, 5. GM09677, 6. GM00232. The uncropped blots and total protein loading controls can be found in the Supplementary File (S3). C) Quantification of lamin A/C levels in tissues from SMA mice and in patient fibroblast cells. In the liver extract, the lower band was presumed to be lamin C, and the upper two bands were presumed to be lamin A isoforms and were consequently measured together to give a single value. The graph is presented as average protein levels in SMA tissues (expressed relative to the control), with error bars showing standard deviation from the mean. The dashed line represents protein levels across healthy control tissues. D) Representative immunohistochemistry images showing lamin A/C staining in the heart from SMA mouse (P8) and healthy age-matched control. Scale bar = 50 μm. Increased lamin A/C staining can be observed in the ventricle wall from SMA mouse, with few lamin A/C positive cells found in the ventricle lumen. E) Densitometry measurements of lamin A/C levels in the ventricle wall are presented as mean optical density, with error bars showing standard

deviation from the mean. F) Lamin A transcript levels in the heart from SMA mice (n = 4) and healthy controls (n = 4) and in fibroblast cells from SMA patients (n = 3) and healthy controls (n = 3). Expression levels of lamin A were normalized to the geometric mean of *POLR2J* and *TBP*. The graphs are presented as mean expression, with error bars showing standard deviation from the mean. CTR- control; ns—not significant; * $p < 0.05$; ** $p < 0.01$; *** $p < 0.001$.

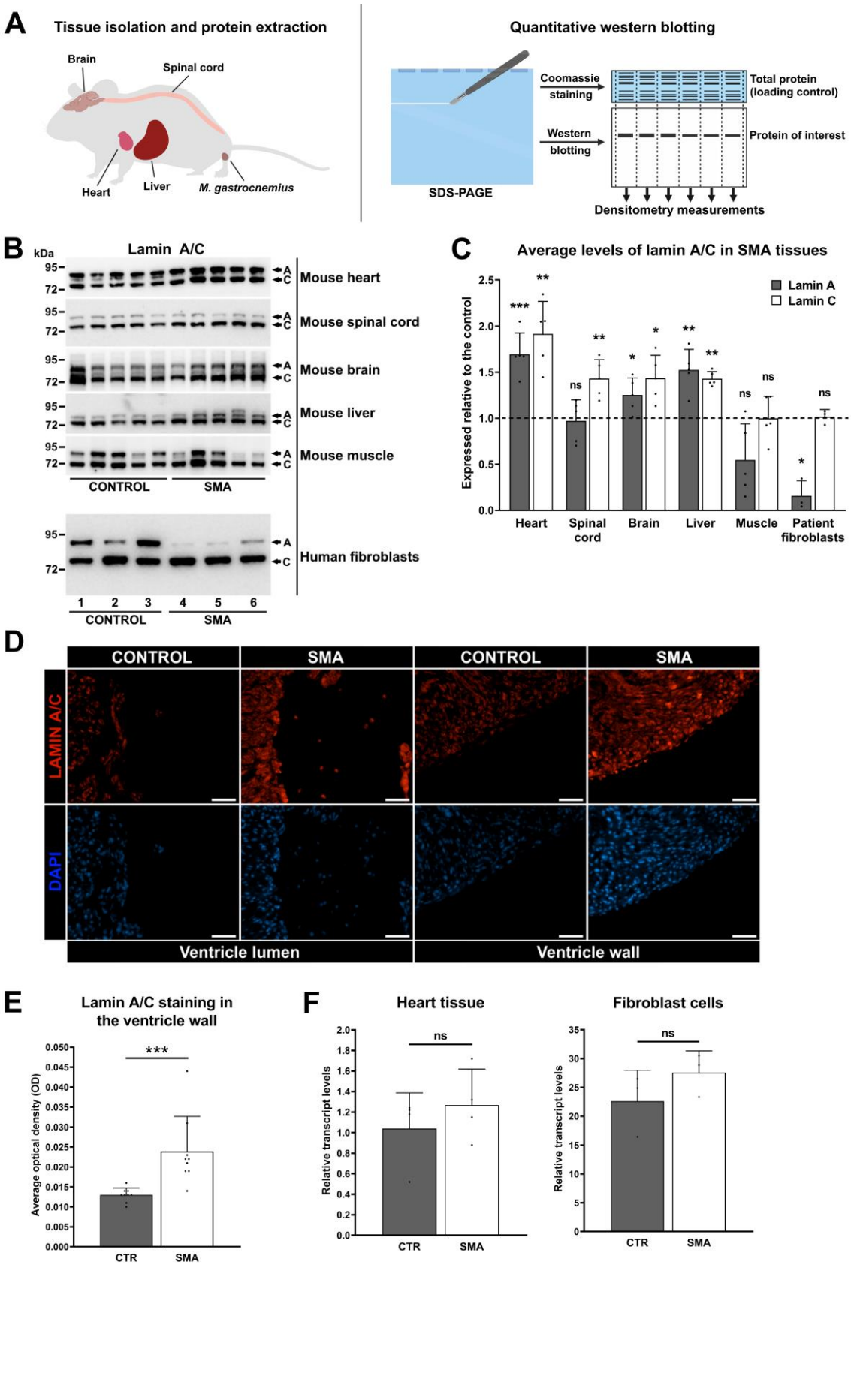

Figure 3. UBA1 and lamin A/C are mechanistically linked

Western blots showing lamin A/C, UBA1 and SMN protein levels in the A) heart, muscle, liver, brain and spinal cord tissue from healthy control mice (n=2) and in fibroblast cells from healthy individuals (n=2), in B) UBA1 KD and control HEK cells (n = 3) and in C) *LMNA* KO and wild type MEFs (n = 3). The uncropped blots and loading controls can be found in the Supplementary File (S5 and S6). Graphs are presented as average protein levels (expressed relative to the control), with error bars showing standard deviation from the mean. The dashed line represents protein levels in control cells. H-heart; M-muscle; L-liver; B-brain; SP-spinal cord; FC-fibroblast cells; ns—not significant; *$p < 0.05$; ** $p < 0.01$; *** $p < 0.001$.

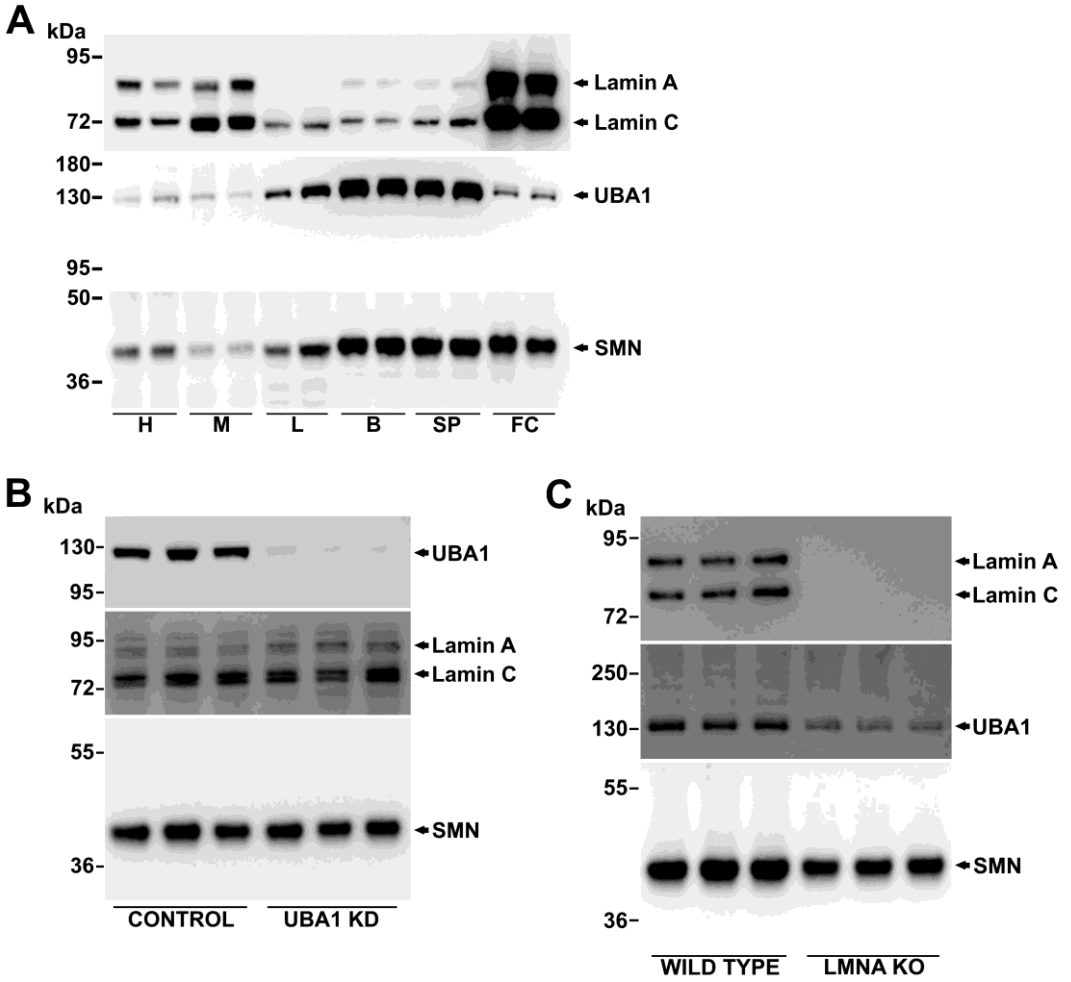

Figure 4. Lamin A/C interacts with β-catenin in mouse heart

A) Representative immunocytochemistry images showing lamin A and UBA1 staining in control and SMA patient fibroblast cells. Arrows in the lower magnification images indicate cells with the most obvious UBA1 staining at the nuclear periphery. Scale bar = 25 μm. Scale bar = 10 μm (control) and 7.5 μm (SMA) in higher magnification images. B) Western blots showing lamin A/C, UBA1 and β-catenin expression in the heart tissue from control and SMA mice after immunoprecipitation with anti-lamin A/C antibody. Beads alone control lanes refer to heart extracts incubated with Dynabeads without the antibody, and represent negative control. #β-catenin band was detected in the eluate from lamin A/C pulldown in both control and SMA samples, but was not observed in the eluate from the beads alone control.

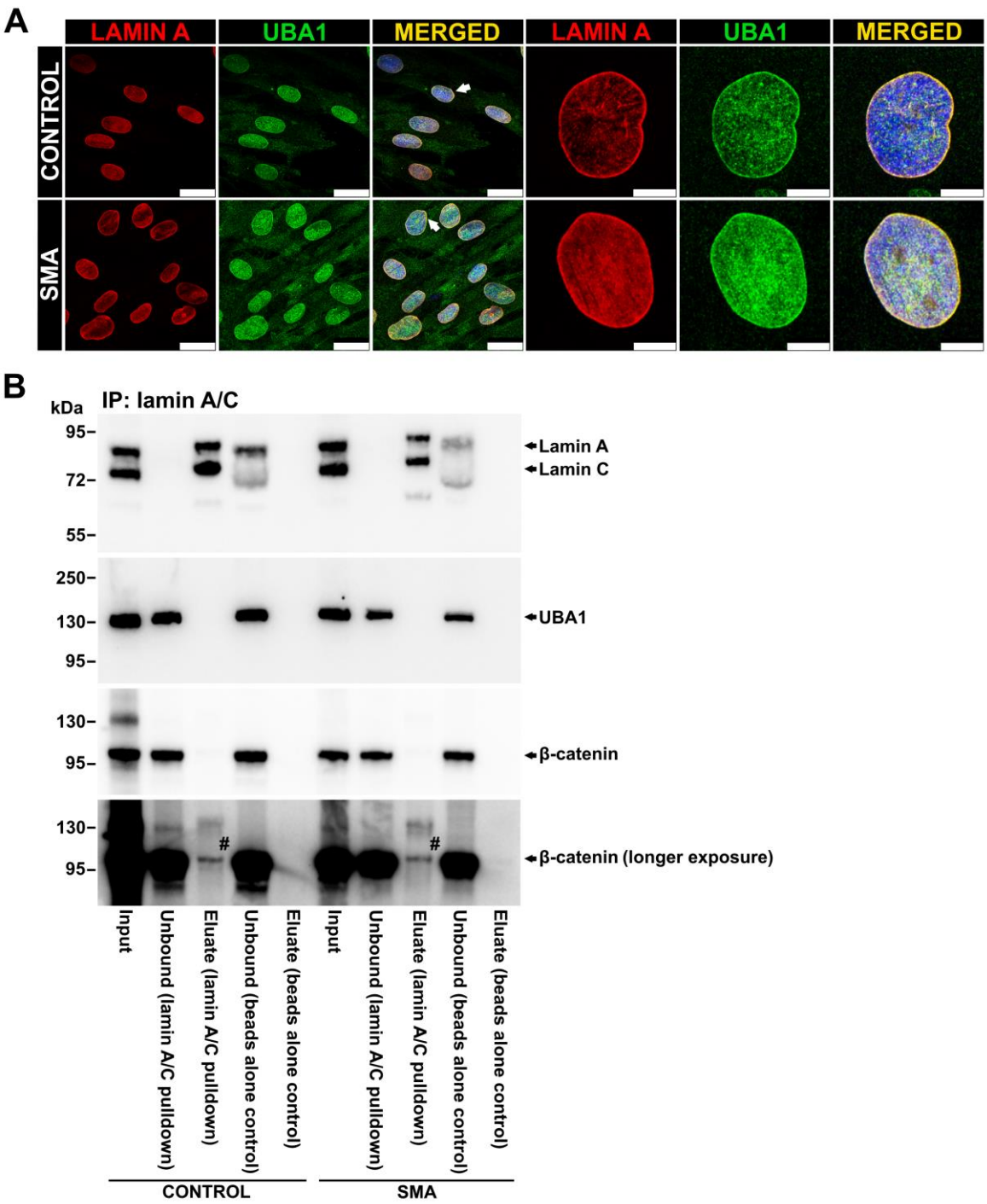

Figure 5. Model of how lamin A/C dysregulation, in combination with other molecular changes, may contribute to cardiac pathology in SMA. A model is proposed in which lamin A/C up-regulation, in combination with other molecular changes that occur in SMA, may lead to cardiac fibrosis and impaired cardiac function. Thinner ventricle walls and dilated ventricles in SMA heart are clinical features of dilated cardiomyopathy. Image created with BioRender.com.

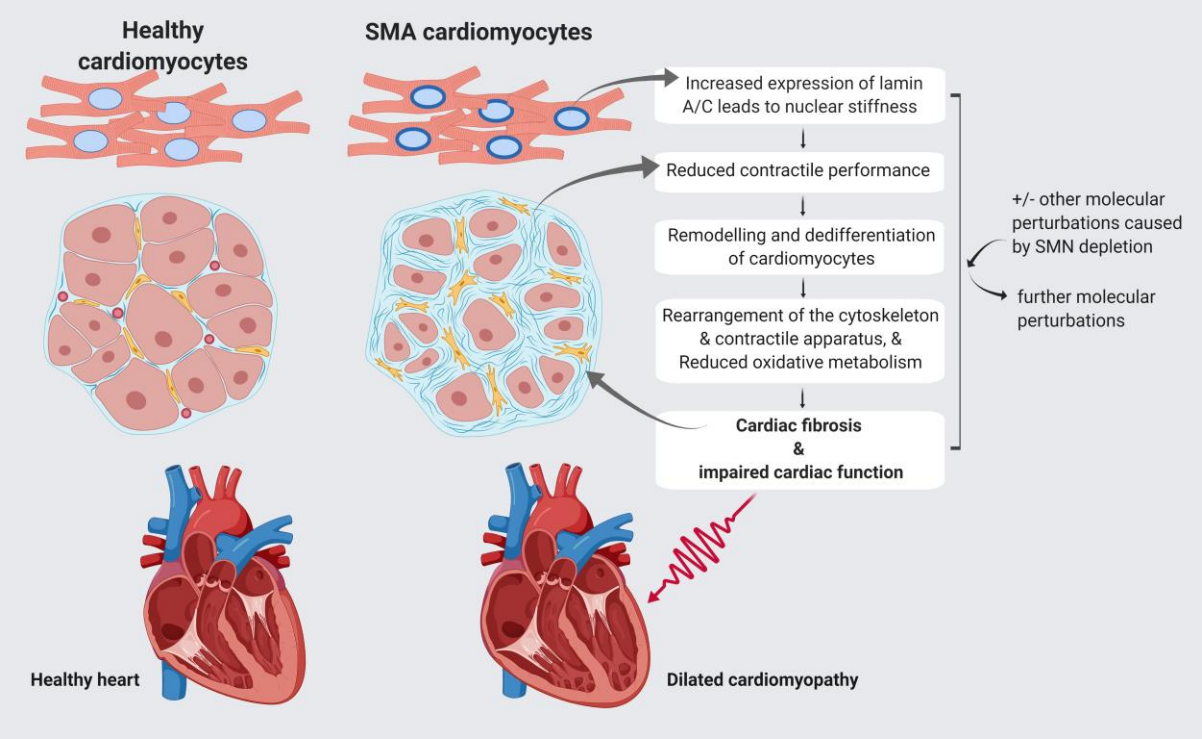

Abbreviations

SMA- spinal muscular atrophy

SMN- survival of motor neuron

SMN1- survival of motor neuron 1, telomeric

SMN2- survival of motor neuron 2, centromeric

LMNA- lamin A/C

ECG- electrocardiogram

iTRAQ- isobaric tags for relative and absolute quantitation

DAVID- database for annotation, visualization and integrated discovery

STRING 10- search tool for the retrieval of interacting genes/proteins

GO- gene ontology

P8-postnatal day 8

RT-qPCR- reverse transcription- quantitative polymerase chain reaction

C_t- cycle threshold

HEK cells - human embryonic kidney cells

MEFs- mouse embryonic fibroblasts

UBA1- ubiquitin like modifier activating enzyme 1

GARS1- glycyl-tRNA synthetase 1

SMAX2- spinal muscular atrophy, x-linked 2

MSCs- mesenchymal stem cells

SUN2- SUN domain-containing protein 2

SUN2- Sad1 and UNC84 domain containing 2

Cdc5l- cell division cycle 5-like protein

RPLC- reverse-phase liquid chromatography

LC-ESI-MS/MS - liquid chromatography-tandem mass spectrometry

OD- optical density

FA- formic acid

DDA- data-dependent acquisition

CE- collision energy

FDR- false discovery rate

PSPEP- Proteomics System Performance Evaluation Pipeline

DMEM- Dulbecco's Modified Eagle Medium

FBS- fetal bovine serum

MEM-NEAA- non-essential amino acids

PEN-STREP- penicillin-streptomycin

KD- knockdown

KO- knockout

SDS-PAGE- sodium dodecyl sulfate- polyacrylamide gel electrophoresis

BSA- bovine serum albumin

PBS- phosphate-buffered saline

NTC- no-template control

POLR2J- RNA polymerase II subunit J

TBP- TATA-Box binding protein

OCT- optimum cutting temperature compound

DAPI- 4',6-diamidino-2-phenylindole